Pueraria protein extract inhibits melanogenesis and promotes melanoma cell apoptosis through the regulation of MITF and mitochondrial-related pathways

YUCHU ZHAO[1*], SHITING YU[1*], YUE WANG[2], YANYAN CHEN[2], JINGJING CHEN[1], JIAWEN WANG[1], MEICHEN LIU[1] and SIMING WANG[1]

[1]Jilin Provincial Key Laboratory of Biomacromolecules of Chinese Medicine, Northeast Asian Research Institute of Traditional Chinese Medicine and [2]College of Pharmacy, Changchun University of Chinese Medicine, Changchun, Jilin 130117, P.R. China

Received August 5, 2022; Accepted December 16, 2022

DOI: 10.3892/mmr.2023.12951

Abstract. *Pueraria Lobata* Radix (*P. Lobata* Radix) is an edible traditional Chinese medicine that contains various active compounds. Proteins from *P. Lobata* Radix have become the subject of increased interest in recent years. In evaluating the whitening effect on the skin, the present study found that the *P. Lobata* Radix water-soluble total protein extract (PLP) had the strongest inhibitory effect on tyrosinase activity. In the present study, the anti-melanogenic effect of PLP and the inhibitory effect on B16 melanoma cells were investigated. PLP significantly reduced the tyrosinase activity and melanin content in B16 melanoma cells. Mechanistically, PLP inhibited melanogenesis by decreasing the expression of tyrosinase, tyrosinase-related protein (TRP)-1 and TRP-2 through downregulation of the microphthalmia-associated transcription factor (MITF) gene, which was mediated by inhibition of p38 mitogen-activated protein kinase signaling. In addition, PLP inhibited cell viability and triggered apoptosis of B16 cells in a dose-dependent manner. Exposure to PLP reduced the mitochondrial membrane potential (MMP) and decreased ATP generation, leading to mitochondria-related apoptosis of B16 melanoma cells. The expression levels of succinate dehydrogenase (SDH) and its two related subunits (SDHA and SDHB) were downregulated significantly by PLP, which may be associated with the regulation of mitochondrial energy metabolism by PLP. These results may explain why MMP collapse and reduced ATP generation were observed in B16 melanoma cells treated with PLP. Finally, the present study demonstrated that the inhibition of melanin synthesis by PLP was correlated with the regulation of antioxidant enzymes to reduce reactive oxygen species levels. These results suggested that PLP inhibits melanogenesis by downregulating the expression of MITF-related melanogenic enzymes and triggering apoptosis through mitochondria-related pathways.

Correspondence to: Dr Meichen Liu or Mr. Siming Wang, Jilin Provincial Key Laboratory of Biomacromolecules of Chinese Medicine, Northeast Asian Research Institute of Traditional Chinese Medicine, Changchun University of Chinese Medicine, 1035 Boshuo Road, Changchun, Jilin 130117, P.R. China
E-mail: liumc0367@163.com
E-mail: lwsm126030@126.com

*Contributed equally

Abbreviations: TRP-1, tyrosinase-related protein 1; TRP-2, tyrosinase-related protein 2; L-DOPA, 3, 4-dihydroxyphenylalanine; MITF, microphthalmia-associated transcription factor; PLP, *P. Lobata* Radix water-soluble total protein; SDHA, succinate dehydrogenase complex A subunit; SDHB, succinate dehydrogenase complex B subunit; WAC, water absorption capacity; OAC, oil absorption capacity; FTIR, Fourier transform infrared absorption spectroscopy; CD, circular dichroism; MTT, thiazolyl tetrazolium; MMP, mitochondrial membrane potential; OCR, oxygen consumption rate; ROS, reactive oxygen species; SDH, succinate dehydrogenase; SOD, superoxide dismutase; CAT, catalase; GSH, glutathione

Key words: Pueraria Lobata protein, melanogenesis, microphthalmia-associated transcription factor, apoptosis, mitochondrial membrane potential

Introduction

Melanin is a ubiquitous biological pigment in plants and animals that absorbs and scatters ultraviolet radiation and reduces free radical production, thus protecting cells from DNA, protein and lipid damage (1,2). Melanin is synthesized on melanosomes in melanocytes, transported to adjacent keratinocytes through dendritic structures and further diffused on the skin surface (3). Hypo- and hyperpigmentation disorders cause serious skin diseases, such as excessive melanin synthesis, which can cause chloasma, freckles and senile plaques (4,5). Therefore, there is significant interest in inhibiting the abnormal synthesis of melanin to treat melanin-related diseases.

Melanogenesis is regulated by tyrosinase, tyrosinase-related protein 1 (TRP-1), TRP-2 and microphthalmia-associated transcription factor (MITF) (6). Tyrosinase catalyzes the hydroxylation of tyrosine into 3,4-dihydroxyphenylalanine

(L-DOPA), which is oxidized to dopa-quinone (7). Tyrosinase catalyzes the rate-limiting step of melanogenesis and TRP-1 and TRP-2 act downstream in the melanin biosynthetic pathway (8). MITF, a basic helix-loop-helix transcription factor, plays a crucial role in melanocyte biology and development by regulating the expression of tyrosinase-related proteins (9,10). MITF expression is enhanced by the activation of melanocyte differentiation (11). Melanocytes that overexpress MITF display high cell proliferation, reduced apoptosis and increased melanin levels when compared with normal melanocytes (12). These cellular features are consistent with the hypothesis that MITF is a master regulator of pigmentation. Expression of the MITF gene is regulated by several signaling pathways, including the p38 MAPK pathway, which is involved in the activation of MITF expression and the consequent increase in tyrosinase expression (13).

Arbutin, kojic acid and ascorbic acid have been reported to possess an inhibitory effect on tyrosinase and act as whitening agents on the skin; however, agents such as kojic acid usually have adverse side effects, including dermatitis and melanocyte damage (14). Therefore, identifying natural compounds with few adverse reactions that target tyrosinase and inhibit melanin synthesis are desirable. *Pueraria Lobata* Radix (*P. Lobata* Radix) belongs to the *Leguminosae* family and contains various active compounds, including flavonoids, isoflavones, proteins and polysaccharides (15). These compounds give *P. Lobata* Radix pharmacological activity, including liver protection and anti-cancer and anti-inflammatory activities (16-18). Proteins from *P. Lobata* Radix have attracted increasing interest in recent years. Using an extracellular screening model, it was found that a *P. Lobata* Radix water-soluble total protein extract (PLP) strongly inhibited tyrosinase activity. As this PLP inhibited tyrosinase and *P. Lobata* Radix has been reported to have anti-cancer activity (19,20), there is interest in investigating the effect of PLP on melanin formation in melanoma.

The present study obtained a PLP by alkali extraction and acid precipitation, characterized the physical and chemical properties of this PLP and evaluated its effect on melanogenesis in B16 melanoma cells. It also analyzed the effect of the PLP on apoptosis in B16 melanoma cells to investigate the potential of this extract as an anti-melanoma agent. The mechanisms by which PLP functions were also investigated. The inhibition of tyrosinase activity and reduction in melanin content by PLP and the related melanogenesis inhibitory mechanism are described here for the first time, to the best of the authors' knowledge.

Materials and methods

Chemicals and reagents. P. Lobata Radix was purchased from Hongjian Pharmacy Co., Ltd. Antibodies against GAPDH (cat. no. BS65483M), tyrosinase (cat. no. BS1484), TRP-1 (cat. no. BS91379), MITF (cat. no. BS6666), Bcl-2 associated X protein (Bax, BS90120), succinate dehydrogenase complex B subunit (SDHB; cat. no. BS8003), phosphorylated (p-)p38 (cat. no. BS6383) and p38 (cat. no. BS60458) were purchased from Biogot Technology Co., Ltd. Antibodies against caspase-3 (cat. no. 9662), caspase-9 (cat. no. 9508), B-cell lymphoma-2 (Bcl-2, #3498) and succinate dehydrogenase complex A subunit (SDHA; cat. no. 11998) were purchased from Cell Signaling Technology, Inc. The antibody against p-MITF (cat. no. PA5-104707) was purchased from Invitrogen (Thermo Fisher Scientific, Inc.). All other reagents and solvents used were of analytical grade. The reactive oxygen species (ROS; cat. no. YX-181519M), superoxide dismutase (SOD; cat. no. YX-191504M), catalase (CAT; cat. no. YX-191518M) and glutathione (GSH; cat. no. YX-181509M) ELISA kits were purchased from Shanghai Youyou Biotechnology Co., Ltd.

Preparation of PLP from dried P. Lobata Radix. Dried *P. Lobata* Radix was ground to powder and passed through a sieve (<0.18 mm). The powder (100 g) was mixed with water (1:10 w/v) and the pH was adjusted to 8.0 by adding dilute NaOH. The sample was incubated at 4˚C for 4 h, centrifuged at 7,000 x g for 10 min at 4˚C and the precipitate was discarded. The pH of the supernatant was adjusted to 3.5 by adding dilute HCl and centrifuged at 7,000 x g for 10 min at 4˚C. The supernatant was then discarded and the remaining sediment lyophilized.

Preparation of PLP from fresh P. Lobata Radix. Fresh *P. Lobata* Radix (100 g) was dispersed in water at a ratio of 1:10 and homogenized. The remaining steps were the same as in the previous section.

Preparation of total flavonoids from P. Lobata Radix. The powder (50 g) obtained from dried *P. Lobata* Radix was extracted by refluxing in 70% (v/v) ethanol (1:40). Extraction was carried out twice for 2 h at 70˚C and the ethanol was removed by evaporation to yield the dried extract.

Preparation of isoflavones from P. Lobata Radix. The powder (50 g) obtained from dried *P. Lobata* Radix was dispersed in 60% (v/v) ethanol (1:20 w/v) and extracted with 300 W ultrasonic power for 60 min at 50˚C. The extraction process was carried out twice. The ethanol fraction was recovered and evaporated to yield the dried extract.

Preparation of P. Lobata Radix water extract. The powder (100 g) obtained from dried *P. Lobata* Radix was extracted twice with water (1:10) for 2 and 1.5 h, respectively. The filtrate was combined and concentrated at 6,000 x g for 10 min at 4˚C and concentrated to a small volume before drying. The obtained *P. Lobata* Radix products were stored in a sealed, dark, dry and cool place.

Tyrosinase inhibition assay. Tyrosine was used as the substrate to detect tyrosinase activity in samples and 3-O-ethyl ascorbate ether was used as the control. In the reaction, 2 mM L-tyrosine (50 μl), 110 μl phosphate buffer (pH 6.8) and 30 μl final samples were mixed and incubated at 37˚C for 10 min. Finally, 50 μl tyrosinase (300 U/ml) was added rapidly to the reaction mixture and incubated for 5 min. The absorbance at 475 nm was measured with a microplate reader (Infinite 200 pro; Tecan Group, Ltd.) every 10 min for at least 1 h.

Determination of water, ash and fat contents of PLP. Moisture determination was carried out according to the National Food Safety Standards GB 5009.3-2016 'Determination of Moisture in Food' (direct drying

method) (https://www.eshian.com/standards/36398.html). Fat levels were determined according to the National Food Safety Standards GB 5009.6-2016 'Determination of Fat in Food' (Soxhlet extraction method) (https://www.eshian.com/standards/37367.html). Ash levels were determined according to the National Food Safety Standards GB 5009.4-2016 'Determination of Ash in Food' (quality method) (https://www.eshian.com/standards/36415.html). The carbohydrate content in samples was determined using the colorimetric phenol-sulfuric acid method according to the previously reported protocol (21).

Determination of surface hydrophobicity of PLP. The surface hydrophobicity was measured using sodium 8-anilino-1-naphthalenesulfonate as the fluorescent probe. PLP solution (1 mg/ml) was diluted with phosphate buffer to a concentration between 0.1-1.0 mg/ml. Diluted PLP solution (4 ml) was mixed with 20 μl 8 mmol/l ANS. The sample was then left standing in the dark for 10 min. The fluorescence intensity of the sample was measured by a fluorophotometer (FL6500; PerkinElmer, Inc.).

Determination of free sulfhydryl and disulfide bond content of PLP. The PLP solution (2 ml) was mixed with 5.0 ml Tris-Gly buffer and 100 μl Ellman reagent (10 mM). After the reaction, the sample was maintained at 25˚C for 15 min and the absorbance at 412 nm was measured. A solution without Ellman reagent was used as a control and Tris-HCl (pH 8.0) was used instead of the sample to determine the baseline value.

The total sulfhydryl content was determined by adding the PLP solution (1.0 ml) to 4.0 ml Tris-Gly-10 mol/l urea and 50 μl Ellman reagent (10 mmol/l). The remaining steps are the same as described for determining the free sulfhydryl content.

Analysis of PLP amino acids. Amino acid standards were prepared by taking 200 μl amino acid mixed standard solution and adding 0.1 mol/l HCl to give a constant volume in a 5 ml volumetric flask. Following dilution, the amino acid sample was used as a standard for testing. Amino acid mixed standard products included 17 standard amino acids.

PLP (30 mg) was dissolved with 20 ml 6 M HCl in a 50 ml hydrolysis tube. The tube was sealed under nitrogen gas and hydrolyzed. After hydrolysis, the tube was cooled to room temperature and the volume was adjusted to 50 ml with ultrapure water. The sample (2 ml) was placed in a vacuum drying oven at 70˚C and evaporated to dryness. The residue was washed and evaporated to dryness twice with the same volume of ultrapure water, diluted with 2.0 ml of 0.02 M HCl, shaken well and filtered through a microporous membrane. A ZORBAX Eclipse Plus C18 (4.6x250 mm; 5 μm; Agilent Technologies, Inc.) column was used for high-performance liquid chromatography analysis. The mobile phase consisted of solvent A (0.1 M methanol) and solvent B (0.1 M sodium acetate buffer). The gradient elution program was: 0-30 min, A 10%; 30-40 min, A 10-35%; 40-50 min, A 35-55%; 50-70 min, A 55-70%; 70-75 min, A 70-10%; 75-78 min, A 10%. The flow rate was 1.0 ml/min, the detection wavelength was 360 nm, the column temperature was 20˚C and the injection volume was 10 μl.

Analysis of PLP by SDS-PAGE. Lyophilized PLP (5 mg) was diluted with distilled water to prepare 1, 3 and 5 mg/ml protein samples. The protein solutions were centrifuged at 12,000 x g for 5 min at 4˚C, the supernatant was collected and a 2X loading buffer was added. The samples were boiled for 5 min to denature proteins and left to cool for later use. Protein electrophoresis was performed and the protein was stained using Coomassie blue staining (cat. no. C8420; Beijing Solarbio Science & Technology Co., Ltd.) and imaged using a gel intelligent imaging system (iBright FL1000; Thermo Fisher Scientific, Inc.).

PLP solubility determination. PLP (1 g) was dissolved in 100 ml of distilled water. The sample was stirred for 20 min (pH set to 1.0-11.0) and incubated at 25˚C for 20 min. The sample was then centrifuged at 3,500 x g for 20 min at 4˚C. The supernatant was tested with the BCA kit (P0012, Beyotime, Shanghai, China) and the test was repeated three times.

Measurement of water absorption capacity (WAC) and oil absorption capacity (OAC) of PLP. PLP (500 mg) was mixed with 2.5 ml of grease in a centrifuge tube and incubated at 25˚C for 30 min. The sample was spun at 3,500 x g for 20 min at 4˚C to remove the upper layer of grease. The weight of the centrifuge tube before and after centrifugation was measured. Using a water-based method, 2.5 ml of oil was required to replace 2.5 ml of distilled water. Finally, WAC or OAC of PLP was characterized by the weight ratio of the centrifuge tubes before and after removing the grease or supernatant.

PLP foamability and foam stability determination. PLP (2 g) was mixed with 200 ml of distilled water (pH adjusted to 2.0, 3.0, 4.0, 5.0, 6.0, 7.0, 8.0, 9.0 and 10.0). The sample was centrifuged at 14,580 x g for 2 min at 4˚C. The foaming volume V_0 at the end of the stirring period was measured. After 30 min (V_{30}), the foaming volume was also measured and the foaming property and foaming stability were calculated. Foaming (%)=V_0/V x100%. Foaming stability (%)=$V_0/V_{30\ x}$ 100%. V is the initial volume.

PLP emulsification and emulsification stability determination. PLP (2 g) was mixed with 200 ml of distilled water (pH adjusted to 2.0, 3.0, 4.0, 5.0, 6.0, 7.0, 8.0, 9.0 and 10.0). Sample (15 ml) and corn oil (5 ml) were added to a tube and stirred at 14,580 x g for 2 min at 4˚C. After stirring, 50 μl of the sample from the bottom of the tube was transferred to a new tube containing 5 ml 0.1% (w/v) SDS. The absorbance at 500 nm was measured using the microplate reader. The emulsification and emulsification stability were calculated. Emulsifying activity (m^2/g)=(2x2.303 x $A_{0\ x}$ DF)/(c x Φ x 10,000). Emulsion stability (min)=($A_{0\ x}$ t)/(A_0-A_t). A_0 is the absorbance value of the sample. A_t is the absorbance value of the sample after standing for 30 min. c is the concentration of the PLP sample. DF is the dilution factor. Φ is the ratio of the oil phase in the emulsion. t is the time.

UV absorption spectrum. An ultraviolet spectrum of the PLP solution was measured over 200-450 nm with an ultraviolet-visible spectrophotometer at room temperature.

Fourier transform infrared absorption spectroscopy (FTIR). After grinding and mixing the freeze-dried PLP powder and dried potassium bromide at a ratio of 1:50, the sample was pressed on a tablet press and scanned in the range 400~4,000 cm^{-1} using a VERTEX 70 infrared spectrometer (Bruker Corporation).

Circular dichroism (CD) spectroscopy. The sample was diluted to 0.2 mg/ml using buffer (20 mM PBS). The standard solution (ultraviolet spectrum, 180-340 nm) and the test samples (far-UV region scan, 190-260 nm) were recorded at room temperature (bandwidth was 1.0 nm, time-per-point was 0.5 sec, pathlength was 0.5 mm and spectra were recorded three times). Pro-Data Viewer software (version 4.5, Applied Photophysics Ltd.) was used to process raw data and CDNN software (version 2.1, Applied Photophysics Ltd.) was used to fit data for calculating the secondary structure of the test protein sample.

Endogenous fluorescence spectroscopy. PLP lyophilized powder was formulated into a 0.1 mg/ml solution using 10 mM phosphate buffer. The pH of the solution was adjusted to 5.0, 7.0 and 9.0 with 1.0 M HCl and 1.0 M NaOH. The excitation wavelength was 280 nm and the fluorescence spectrum with a wavelength range of 300-500 nm was recorded. The excitation and emission slit width was 5 nm.

Cell culture. The mouse melanoma cell line (B16 cells) was obtained from the Type Culture Collection of the Chinese Academy of Sciences and cultured in RPMI 1640 medium (cat. no. SH30809.01) supplemented with 10% fetal bovine serum (cat. no. SV30208), 1% penicillin and streptomycin (cat. no. SV30010; all from HyClone; Cytiva). Cells were cultured in a humidified normoxic chamber (Thermo Fisher Scientific, Inc.) with 5% CO_2 at 37˚C.

Cell viability assay. B16 cells were seeded in 96-well plates ($3x10^3$ cells/well) and cultured for 24 h. The medium was then replaced with fresh medium containing PLP at various concentrations (0.1, 0.3 and 0.5 mg/ml) for 48 h at 37˚C. Thiazolyl tetrazolium (MTT; 5 mg/ml) was added to each well and incubated in darkness at 37˚C for 4 h. MTT is a yellow compound that acts on the mitochondria of living cells to produce blue formazan crystals. The resulting formazan crystals were dissolved in 150 μl DMSO and the absorbance at 490 nm was recorded using a microplate reader. Cell viability (%)=$(A_{sample}-A_{blank})/(A_{control}-A_{blank})$ x100%. The EC_{50} value was calculated using GraphPad Prism 6.0 software (Dotmatics).

Assay of melanin content. B16 cells were seeded into 6-well plates at a density of $6x10^4$ cells/well and treated with or without PLP (0.1, 0.3, 0.5 mg/ml) at 37˚C for 48 h. After removing the medium, the cells were washed twice with PBS and harvested by centrifuging at 530 x g for 5 min at room temperature. The cells were then lysed by incubation in 1 M NaOH [10% (v/v) DMSO] at 60˚C for 1 h. The amount of melanin was determined spectrophotometrically immediately after lysis by measuring the absorbance at 475 nm using a microplate reader. The melanin content in control wells was set as 100% and the results were expressed as percentages of the control wells. The assay was repeated at least three times.

Cellular tyrosinase activity assay. Tyrosinase enzyme activity was estimated by measuring L-DOPA oxidation. Briefly, the method to culture B16 cells was the same as aforementioned. The cells were washed twice with PBS, mixed with 1% Triton X-100 and cryopreserved at -80˚C for 30 min. The cells were lysed at room temperature, heated in water at 37˚C for 5 min and mixed with 200 μl of 0.1% (w/v) L-DOPA at 37˚C for 2 h. The absorbance was measured at 475 nm using a microplate reader every 10 min for at least 1 h. Tyrosinase activity was expressed as percentages of activity in untreated cells.

Reverse transcription-quantitative PCR (RT-qPCR). Total RNA was extracted from $1x10^6$ B16 cells using a total RNA extraction kit (DP424; Tiangen Biotech Co., Ltd.), according to the manufacturer's instructions and reverse transcription was performed according to Prime Script RT Reagent kit instructions (DRR047A; Takara Bio, Inc.). Aliquots of cDNA were subjected to qPCR analysis with SYBR Green PCR Master Mix (cat. no. DRR420A; Takara Biotechnology) and a Real-Time PCR system equipped with a CFX 96 Connect Optics Module (Bio-Rad Laboratories, Inc.). Program was: 94˚C pre-denaturation for 30 sec; 40 cycles (94˚C denaturation for 5 sec, 60˚C annealing for 1 min). Expression levels of target genes were normalized to the GAPDH gene expression level using the $2^{-\Delta\Delta Cq}$ method (22). All assays were performed in triplicate. The primer sequences are listed in Table I.

Western blotting. Cells were washed twice with PBS, centrifuged at 530 x g and 4˚C for harvesting and lysed with RIPA lysis buffer (P0013C; Beyotime). Total protein was measured using a BCA kit (P0010S; Beyotime Institute of Biotechnology). Proteins (20 μg/lane) were separated by 12% SDS-PAGE and transferred onto a nitrocellulose membrane by semidry blotting. Non-specific protein binding was blocked by incubating the membranes with 5% (v/v) non-fat dried milk (P0216; Beyotime Institute of Biotechnology) in PBS at 25˚C for 1 h and the membranes were then incubated overnight at 4˚C with primary antibodies as follows: GAPDH (1:1,000), tyrosinase (1:1,000), TRP-1 (1:1,000), MITF (1:1,000), Bax (1:1,000), SDHB (1:1,000), p-p38 (1:1,000), p38 (1:500), caspase-3 (1:1,000), caspase-9 (1:1,000), Bcl-2 (1:1,000), SDHA (1:1,000) and p-MITF (1:1,000). Following washing with PBS containing 0.05% (v/v) Tween-20 (P1033; Bejing Solarbio Science & Technology Co., Ltd.) (PBST), the membranes were incubated with horseradish peroxidase-conjugated anti-mouse IgG (cat. no. BS12478; 1:5,000; Biogot Tech) or horseradish peroxidase-conjugated anti-rabbit IgG (cat. no. BS13278; 1:5,000; Biogot Tech) for 1 h at 25˚C and bands were visualized using Enhanced Chemiluminescence Reagent kit (cat. no. P0018FS; Beyotime Institute of Biotechnology). Membranes were imaged using the iBright FL1000 Imaging System. Image J software 1.53a (National Institutes of Health) was used to quantify the gray value of western blot bands and the protein expression level was normalized as the gray value of the target protein/loading control protein.

Table I. Primer sequences used in the present study.

Gene	Gene ID	Accession number	Forward (5'-3')	Reverse (5'-3')
GAPDH	14433	NM_001289726.2	TGCCCAGAACATCATCCCT	TGAAGTCGCAGGAGACAACC
Bax	12028	NM_001411994.1	GGAGATGAACTGGATAGCAA TATGG	GTTTGCTAGCAAAGTAGAAGA GGGCG
Bcl-2	12043	NM_009741.5	CTGGCATCTTCTCCTTCCAG	GACGGTAGCGACGAGAGAAG
MITF	17342	NM_001113198.2	CAACGGGAACAGCAACGAGC	CGGTGGATGGGATAAGGGAAA
Tyrosinase	22173	NM_001317397.1	GAACACCTGAGGGACCAC	CATTGGCTTCTGGGTAAA
TRP-1	22178	NM_001282014.1	CATAACAGGCAATACAACAT	GTAACAACGCAGCCACTA
TRP-2	13190	NM_010024.3	CCCCTTTCGCCACAGCCCAA CT	GCGGTCCTCAGACTCTTCCACA TTCC
p38	26416	NM_001168508.1	GGGAGGTGCCCGAACGATAC	TGGCGTGAATGATGGACTGAAA

Cell apoptosis analysis. The apoptosis incidence was determined by an Amnis Flow Sight flow cytometer (Merck & Co., Inc.) using the Annexin V-FITC Apoptosis Detection kit (cat. no. 556547; BD Biosciences). Briefly, B16 cells were incubated with fresh medium (as control) or medium containing PLP for 48 h at 37˚C. After treatment, the cells were collected by centrifugation at 303 x g for 5 min at 24˚C, washed twice with ice-cold PBS, suspended in 1X Binding Buffer and incubated with 5 μl each of propidium iodide (PI) and Annexin V-FITC solutions. Probes were incubated in darkness at 37˚C for 15 min. Samples were examined with a flow cytometer and quantified using Amnis IDEAS software v6.1 (Merck & Co., Inc.). The number of total apoptotic cells, including early and late apoptotic cells, was counted and represented as percentages of the total cell count.

Mitochondrial membrane potential (MMP) assessment. MMP changes in B16 cells were measured by rhodamine-123 staining (cat. no. C2008S; Beyotime Institute of Biotechnology). Briefly, treated cells were trypsinized, washed with PBS and stained with rhodamine-123 in darkness at 37˚C for 30 min. After centrifugation (430 x g at room temperature for 5 min), the cells were resuspended in 300 μl PBS and staining was measured by the Amnis Flow Sight flow cytometer (Merck & Co., Inc.) at an excitation wavelength of 507 nm and a maximum emission wavelength of 529 nm.

Mitochondrial fluorescence photography. B16 cells were incubated with fresh medium (as control) or medium containing PLP for 48 h at 37˚C. The cell culture medium was removed, Mito-Tracker Green (cat. no. C1048; Beyotime Institute of Biotechnology) was added and the cells were incubated in darkness at 37˚C for 30 min. Mito-Tracker Green was removed and 1 ml Hoechst 33342 staining solution (cat. no. C1022; Beyotime Institute of Biotechnology) was added. The cells were washed twice again after labeling in darkness at 37˚C for 10 min and then observed with an EVOS® FL Auto Imaging System (Thermo Fisher Scientific, Inc.).

Measurement of oxygen consumption rate (OCR). OCR, as a surrogate indicator of mitochondrial oxidative phosphorylation, were measured with the Seahorse Cell Mitochondrial Stress Test kit (cat. no. 103010-100; Agilent Technologies, Inc.). In brief, control or PLP-treated B16 cells were harvested to detect OCR, including basal OCR, ATP-linked OCR, reserve capacity OCR and proton leak OCR, after the administration of oligomycin (Complex V inhibitor, 1 μM), carbonyl cyanide 4-(trifluoromethoxy)-phenylhydrazone (0.5 μM; an uncoupling agent of mitochondrial respiration to achieve the maximal respiration rate) and rotenone/antimycin A (Complex I/III inhibitor, 0.5 μM) in a Seahorse XFp Analyzer (Agilent Technologies, Inc.). The OCR was displayed as pmol/min.

Measurement of intracellular ATP levels. Intracellular ATP concentrations were assayed with an ATP assay kit (cat. no. S0026; Beyotime Institute of Biotechnology) according to the manufacturer's instructions. Briefly, 200 μl ice-cold ATP lysis buffer was added to cells and the cell lysate was harvested at 12,000 x g and 4˚C for 10 min. The supernatant was taken and the reaction started at 37˚C for 3 min, by adding 100 μl ATP detection buffer to deplete background ATP and then adding 10 μl supernatant for detection. Relative light unit (RLU) values were recorded by the microplate reader.

ROS and oxidative stress marker analysis. The ROS content, SOD, CAT and GSH in B16 cells was detected by ELISA. Cells were harvested and ruptured by repeated freeze-thaw steps. The sample was then centrifuged at 3,000 x g and 4˚C for 10 min and the supernatant was taken for testing. Reagents were added according to the kit method and samples were incubated at 37˚C for 60 min. After adding the color reagent, the samples were incubated in darkness at 37˚C for 15 min. Finally, 50 μl stop solution was added and the absorbance at 450 nm was measured within 15 min using the microplate reader.

Statistical analysis. Data were evaluated using GraphPad software (version 9; GraphPad Software; Dotmatics). Data were presented as the mean ± standard deviation of three independent experiments and were analyzed by one-way ANOVA and Dunnett's post-hoc test. $P<0.05$ was considered to indicate a statistically significant difference.

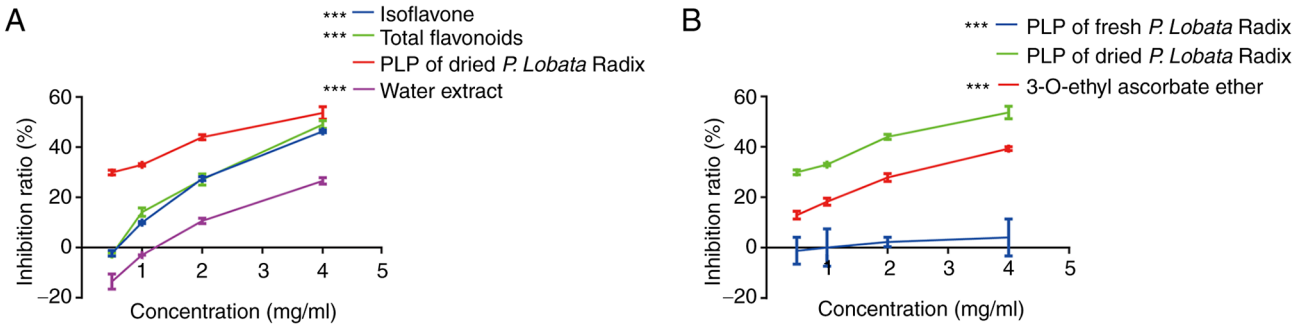

Figure 1. Determination of tyrosinase activity using different extraction methods of *P. Lobata* Radix. (A) The tyrosinase inhibition rates of dried *P. Lobata* Radix extracts contained isoflavone, total flavonoids, PLP and water extract. (B) Comparison of the tyrosinase activity inhibition rate of PLP extracted from dried and fresh *P. Lobata* Radix, with 3-O-ethyl ascorbate ether used as the positive control. PLP, *P. Lobata* Radix water-soluble total protein extract. ***P<0.001 vs. PLP of dried *P. Lobata* Radix.

Results

Inhibitory effect of P. Lobata Radix extracts on tyrosinase activity. Tyrosinase is a copper-containing and rate-limiting enzyme that regulates melanin biosynthesis (23). The present study first screened different *P. Lobata* Radix extracts for inhibition of tyrosinase activity using a spectrophotometric assay. Tyrosinase inhibition results for different dried *P. Lobata* Radix extracts showed that PLP had the strongest inhibitory effect on tyrosinase with an IC_{50} of 4.0 mg/ml (Fig. 1A).

In addition, the tyrosinase inhibition rates of PLP extracted from fresh *P. Lobata* Radix and dried *P. Lobata* Radix were compared. The result showed that dried *P. Lobata* Radix inhibition of tyrosinase was concentration-dependent and stronger than the inhibition observed for proteins from fresh *P. Lobata* Radix and the positive control (3-O-ethyl ascorbate ether) (Fig. 1B). Thus, we used dried *P. Lobata* Radix in subsequent experiments. These results indicated that PLP is a potential tyrosinase inhibitor.

Analysis of the properties of PLP. The analysis of PLP showed that the protein content was 90.17% (Table II). The surface hydrophobicity was 457, the free sulfhydryl content was 6.45 μmol/g, the total sulfhydryl content was 12.65 μmol/g and the disulfide bond content was 3.1 μmol/g (Table III). The leucine content was the highest of the essential amino acids at 3.05/100 g, whereas the aspartic acid content was the highest of the non-essential amino acids at 3.51/100 g (Table IV).

Chemical characterization of PLP. Separation by SDS-PAGE showed that PLP was composed of 11 proteins (Fig. 2A). As shown in Fig. 2B, at pH 3.0, the solubility of PLP was the lowest when the isoelectric point was reached. The solubility of PLP increased gradually with increasing pH, with the highest solubility at pH 8.0. WAC and OAC experiments revealed that there are more hydrophobic than hydrophilic groups in PLP (Fig. 2C). The foaming ability of PLP was highest when the pH was 7.0 and the foaming stability was found to be highest at pH 5.0 (Fig. 2D). The emulsifying activity and stability of PLP were the lowest when the pH reached the isoelectric point (Fig. 2E). With increasing pH, the emulsifying activity of PLP gradually increased and the emulsifying stability reached a maximum at pH 6.0.

Spectral analysis of PLP. The UV spectrum of PLP had absorption peaks at ~257 and 280 nm (Fig. 3A). PLP has a number of characteristic absorption peaks in the FTIR spectrum (Fig. 3B). For example, the amide I band (1,600-1,700 cm^{-1}) contains abundant secondary structure information on proteins, with the 1,634 cm^{-1} peak indicating proteins with β-sheet secondary structure and the amide III band (1,220-1,330 cm^{-1}) suitable for distinguishing between α-helix secondary structure and random coil. The peak at 1,263 cm^{-1} in the FTIR spectrum arises from protein with random coil. The infrared spectroscopic results were consistent with the CD spectrum and the secondary structure of PLP was analyzed using this spectrum (Fig. 3C and Table V). The CD results for PLP showed a negative peak near 198 nm and a small and broad positive peak near 202 nm, indicative of random coil. The endogenous fluorescence spectrum showed that the fluorescence intensity of PLP decreased with increasing pH. In addition, changing the pH yielded a minor redshift effect (Fig. 3D).

Effect of PLP on cellular melanin synthesis in mouse melanoma B16 cells. Cell viability was first evaluated to determine the effects of PLP on cellular melanin synthesis. The MTT assay revealed that the proliferation of B16 melanoma cells decreased significantly as the concentration of PLP increased (78.40±3.03, 62.56±6.81 and 45.82±6.99%) and the EC_{50} of PLP was 0.35 mg/ml (Fig. 4A). To examine the effects of PLP on melanogenesis, a melanin content assay was performed in mouse melanoma B16 cells. As shown in Fig. 4B, treatment with PLP decreased the melanin content in B16 melanoma cells in a dose-dependent manner (84.41±1.99, 63.22±2.11, 49.32±7.69%). In addition, cellular tyrosinase activity was also suppressed by PLP treatment in a dose-dependent manner (47.00±3.22, 28.70±2.46 and 21.43±1.20%; Fig. 4C). These data indicated that PLP inhibited tyrosinase activity and had an inhibitory effect on melanocytes, suggesting that PLP may be a good whitening agent at the molecular and cellular levels.

Effect of PLP on melanogenesis-related gene expression. RT-qPCR and western blot analyses were performed to investigate the effects of PLP on the expression of melanogenesis-related genes. The mRNA expression levels of MITF and its downstream genes, tyrosinase, TRP-1 and TRP-2, all decreased as the concentration of PLP increased (Fig. 5A). In

Table II. Water, ash, protein, carbohydrate and fat content of PLP

Index	Content (%)
Moisture	3.1±0.1
Ash	0.51±0.2
protein	90.17±0.06
carbohydrate	6.14±0.73
Fat	0.09±0.01

PLP, *P. Lobata* Radix water-soluble total protein.

Table III. PLP hydrophobicity and sulfur content

Index	PLP
Surface hydrophobicity	457±16.77
Free sulfhydryl content (μmol/g)	6.45±0.6
Total sulfhydryl content (μmol/g)	12.65±0.83
Disulfide bond (μmol/g)	3.1±0.53

PLP, *P. Lobata* Radix water-soluble total protein.

Table IV. PLP amino acid content

A, Essential amino acids

Amino acids	PLP (g/100 g)
Histidine (His)	0.73±0.003
Isoleucine (Ile)	1.54±0.03
Leucine (Leu)	3.05±0.07
Lysine (Lys)	1.85±0.04
Methionine (Met)	0.29±0.01
Phenylalanine (Phe)	1.93±0.03
Threonine (Thr)	1.91±0.04
Valine (Val)	2.50±0.06

B, Non-essential amino acids

Amino acids	PLP (g/100 g)
Aspartic (Asp)	3.51±0.06
Glutamic (Glu)	3.09±0.07
Serine (Ser)	1.49±0.05
Cystine (Cys)	0.27±0.01
Glycine (Gly)	1.90±0.04
Tyrosine (Tyr)	1.22±0.04
Arginine (Arg)	1.53±0.04
Alanine (Ala)	1.10±0.02
Proline (Pro)	1.90±0.04

PLP, *P. Lobata* Radix water-soluble total protein.

addition, treatment with PLP markedly inhibited the protein expression levels of p-MITF, MITF, tyrosinase and TRP-1 in B16 melanoma cells and did not affect the p-MITF/MITF ratio (Fig. 5B-G). These findings indicated that the inhibitory effects of PLP on melanogenesis in B16 melanoma cells may be mediated by the downregulation of MITF-related melanogenic genes.

The expression of the MITF gene is regulated by p38 MAPK. For this reason, the effect of PLP on the expression of p38 was examined. As shown in Fig. 5H-K, PLP decreased the mRNA level of p38 and protein expression levels of p-p38 and p38 significantly, but did not affect the p-p38/p38 ratio, which were consistent with the expression of MITF. These results suggested that p38 MAPK operates upstream of MITF in PLP-regulated melanogenesis.

Effect of PLP on the apoptosis of mouse melanoma B16 cells. MITF-overexpressing melanocytes showed reduced apoptosis and increased melanin levels when compared with normal melanocytes (24). The results of the present study indicated that PLP inhibited the expression of the MITF gene in melanoma B16 cells and it was hypothesized that PLP induced cell apoptosis. Thus, apoptosis in B16 cells was examined by Annexin V-FITC/PI staining and flow cytometry to investigate the effect of PLP. As shown in Fig. 6A and B, the percentage of apoptotic cells in the control group was 7.33±1.23%. As the concentration of PLP increased, the apoptosis rate of B16 melanoma cells increased gradually (17.18±3.57, 39.73±14.67 and 55.60±11.96%).

Effect of PLP on mitochondrial apoptotic pathways. Mitochondria play a central role in the growth and apoptosis of cells (25). To determine whether mitochondrial apoptotic signaling pathways are potentially involved in PLP-induced apoptosis, the expression levels of a pro-apoptotic protein (Bax), anti-apoptotic protein (Bcl-2), caspase-3 and caspase-9 were evaluated. The results showed that B16 cells treated with PLP had higher Bax expression and lower Bcl-2 expression (Fig. 7A-D) and the expression levels of procaspase-3 (Fig. 7E) and procaspase-9 were also upregulated significantly when compared with untreated cells (Fig. 7F). Thus, PLP-induced apoptosis might be related to mitochondrial apoptotic signaling pathways.

PLP-induced mitochondrial dysfunction in mouse melanoma B16 cells. The role of mitochondria in PLP-induced apoptosis of melanoma B16 cells was further elucidated by detecting the MMP and mitochondria of live cells by flow cytometry and Mito-Tracker probes, respectively. Compared with control cells, the MMP of cells treated with PLP was reduced significantly and the MMP decreased gradually as the concentration of PLP increased (Fig. 8A). In addition, Hoechst was used to locate cells and Mito-Tracker was used to stain the mitochondria of live cells specifically. The results showed that the green fluorescence gradually weakened (Fig. 8B and C).

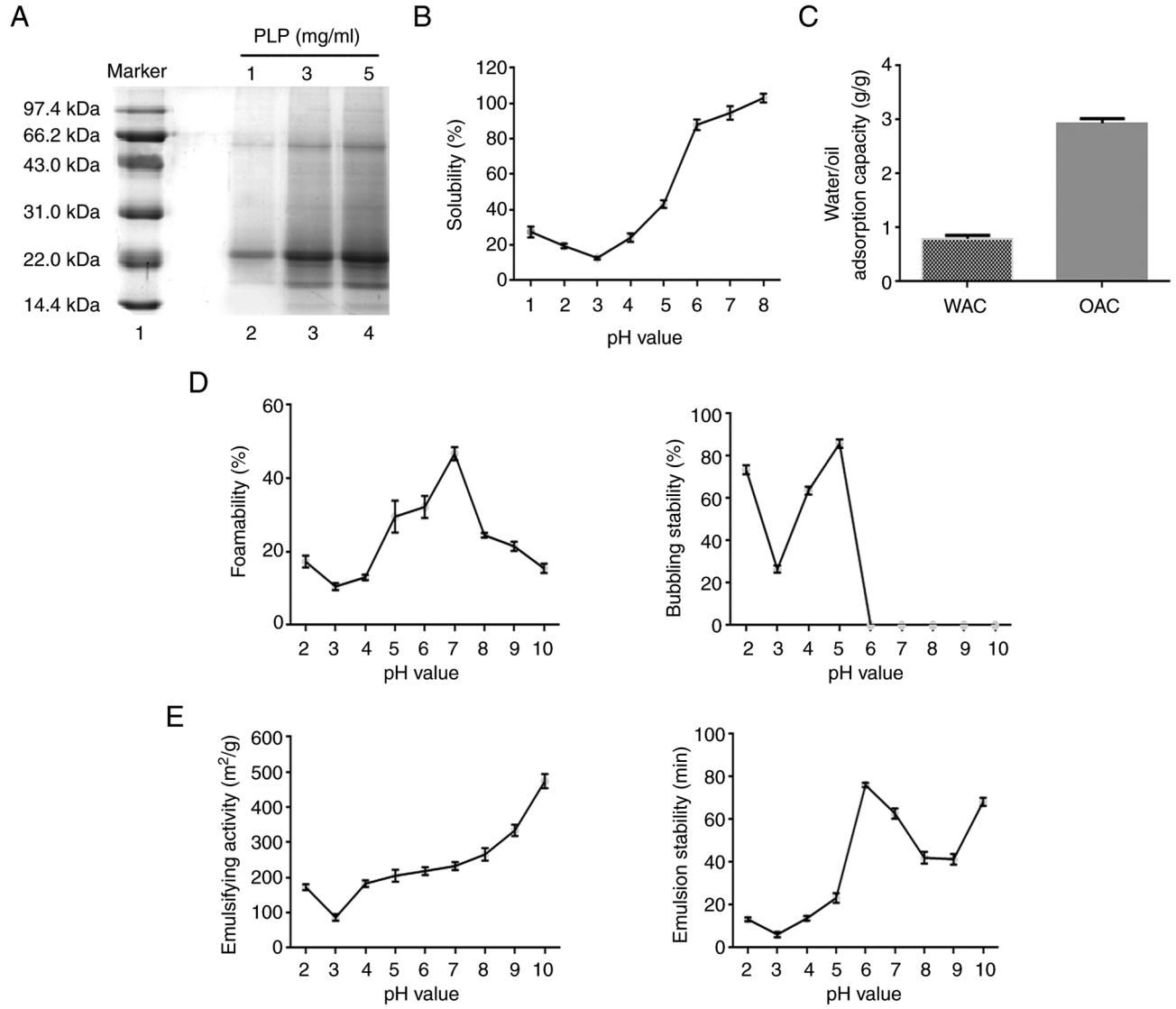

Figure 2. Chemical characterization of PLP. (A) Electrophoretic analysis of PLP. (B) Solubility changes of PLP under different pH conditions. (C) WAC and OAC of PLP. (D) Effects of different pH conditions on foamability and foaming stability of PLP. (E) Effect of different pH conditions on the emulsification activity and stability of PLP. PLP, *P. Lobata* Radix water-soluble total protein extract; WAC, water absorption capacity; OAC, oil absorption capacity.

Effect of PLP on mitochondrial energy metabolism and ATP generation. Mitochondrial energy metabolism is essential for the ability of cells to maintain the MMP (4). A Seahorse XFp extracellular flux analyzer was used to study the effect of PLP on mitochondrial energy metabolism. Experiments monitoring mitochondrial energy metabolism evaluated mitochondrial oxygen utilization buffer capacity, oxygen consumption and other functions (26). Under normal conditions, melanoma cells display a high rate of mitochondrial energy metabolism (27). The rate of tumor cell metabolism decreased after treatment with PLP and a concentration of 0.5 mg/ml PLP had the strongest effect (Fig. 9A and B). PLP treatment reduced OCR significantly, which was linked to ATP production (Fig. 9C-F). Similarly, PLP also decreased the levels of ATP in treated cells (Fig. 9G).

Effect of PLP on succinate dehydrogenase. Mitochondrial energy metabolism and MMP have been shown previously to decrease in a concentration-dependent manner after treatment with PLP. However, the cause of the decrease has remained unresolved. Therefore, an ELISA assay was used to detect changes in SDH and protein levels of its two related subunits. The results showed that the content of SDH decreased after treatment with PLP (Fig. 10A) and the levels of its two related subunit proteins also decreased simultaneously (Fig. 10B-D). Treatment with 0.5 mg/ml PLP had the strongest effect.

Effect of PLP on intracellular ROS levels and oxidative stress. Melanin synthesis involves an oxidation reaction and is important for ROS generation and hyperpigmentation. The present study investigated the correlation between the inhibition of melanogenesis and the antioxidant activity of PLP. The level of ROS in cells decreased significantly when cells were incubated with PLP (Fig. 11A) and the activities of SOD (Fig. 11B), CAT (Fig. 11C) and GSH (Fig. 11D) increased significantly. The results suggested that the inhibitory effect of PLP on melanin synthesis may also be related to an antioxidant effect.

Table V. PLP secondary structure.

Secondary structure	190-260 nm (%)	195-260 nm (%)	200-260 nm (%)	205-260 nm (%)	210-260 nm (%)
α-helix	7.1	7.6	6.5	4.7	5.4
β-sheet	40.7	37.1	39.2	40.8	44.9
β-turn	22.7	23.6	25.3	23.5	19.4
Random curl	31.6	34.5	38.3	35.0	35.2
Total	102.2	102.8	109.4	104.0	104.9

PLP, *P. Lobata* Radix water-soluble total protein.

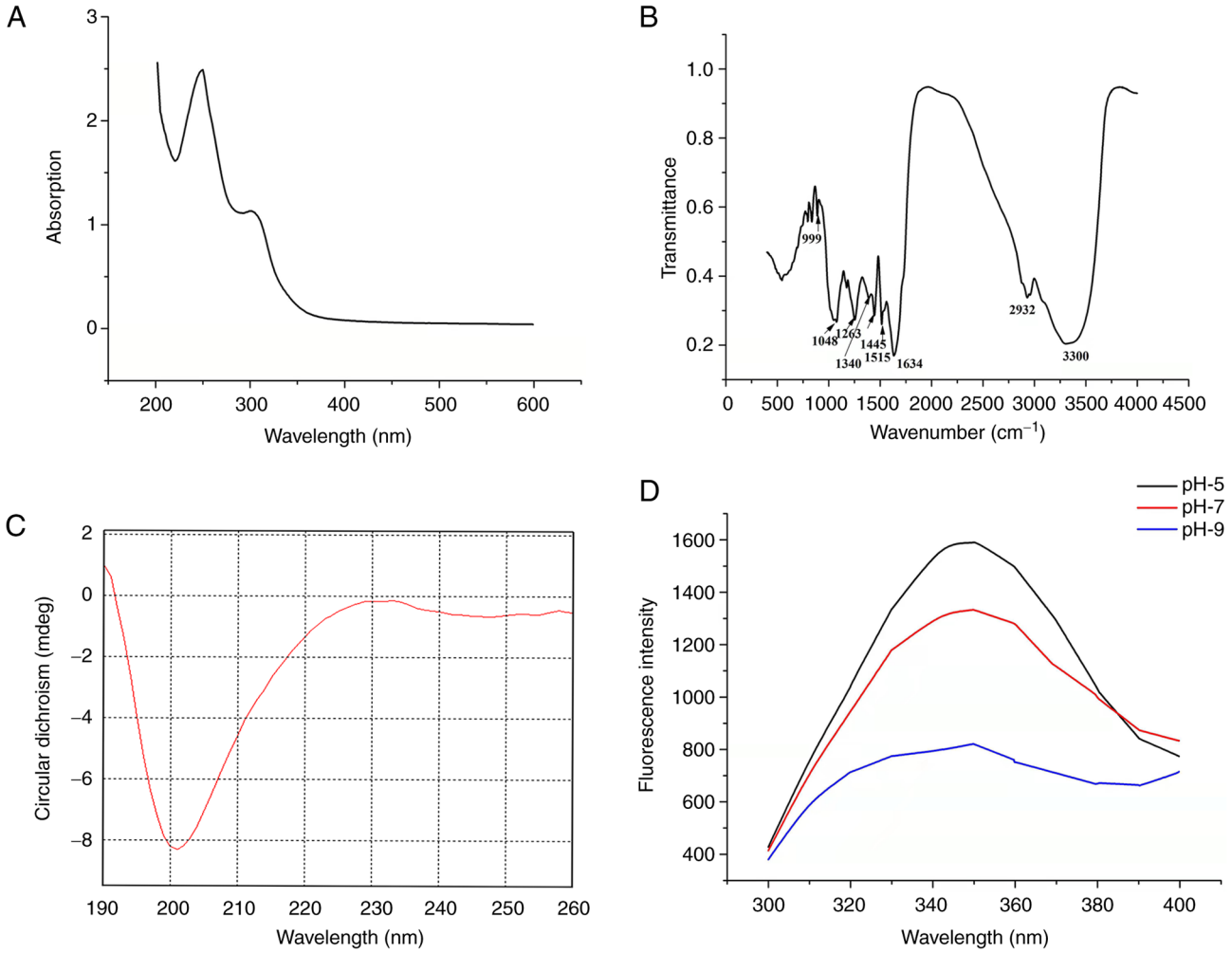

Figure 3. Spectral analysis of PLP. (A) UV spectrum, (B) Fourier transform infrared absorption spectroscopy spectrum, (C) Circular dichroism spectrum and (D) endogenous fluorescence spectrum of PLP. PLP, *P. Lobata* Radix water-soluble total protein extract.

Discussion

PLP was shown to inhibit melanin synthesis in B16 melanoma cells. PLP is rich in amino acids, including eight essential amino acids: His, Ile, Leu, Lys, Met, Phe, Thr and Val, and nine non-essential amino acids: Asp, Glu, Ser, Cys, Gly, Tyr, Arg, Ala and Pro. PLP exhibited good solubility, foamability, foaming stability, emulsification activity and emulsification stability under different pH conditions. In addition, spectroscopic analysis provided structural information on PLP. The effect of PLP on melanogenesis in B16 melanoma cells was attributed to the inhibition of cellular tyrosinase activity. PLP inhibited melanogenesis by decreasing the expression of tyrosinase, TRP-1 and TRP-2 through downregulation of the MITF gene, which was mediated by inhibition of p38 MAPK signaling. In addition, PLP significantly inhibited cell viability and induced apoptosis in B16 melanoma cells. Exposure to PLP altered the mitochondrial function in

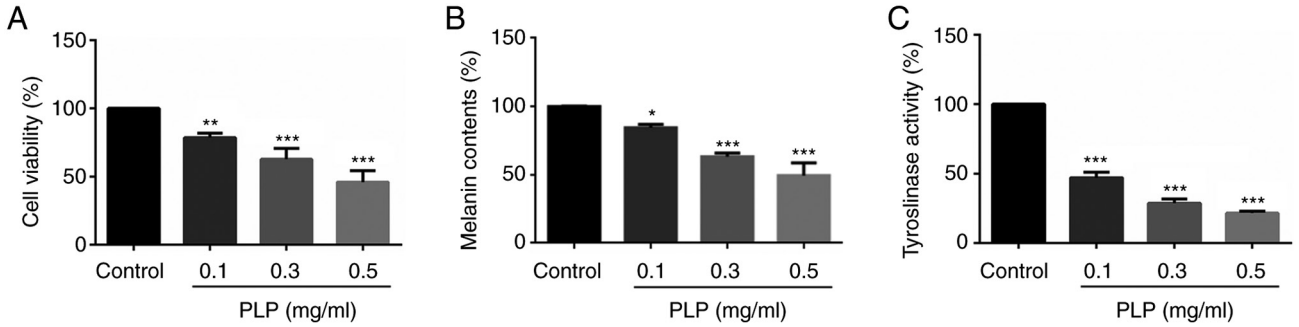

Figure 4. Effects of PLP on B16 cell viability, melanin synthesis and tyrosinase activity. (A) The cellular viability of B16 cells was determined by the MTT assay after PLP treatment for 48 h. (B) Effect of PLP on melanin content in B16 cells. The melanin content was expressed as a percentage of the control. (C) Inhibitory effect of PLP on tyrosinase activity in B16 cells. *P<0.05, **P<0.01 and ***P<0.001 vs. control. PLP, *P. Lobata* Radix water-soluble total protein extract; MTT, thiazolyl tetrazolium.

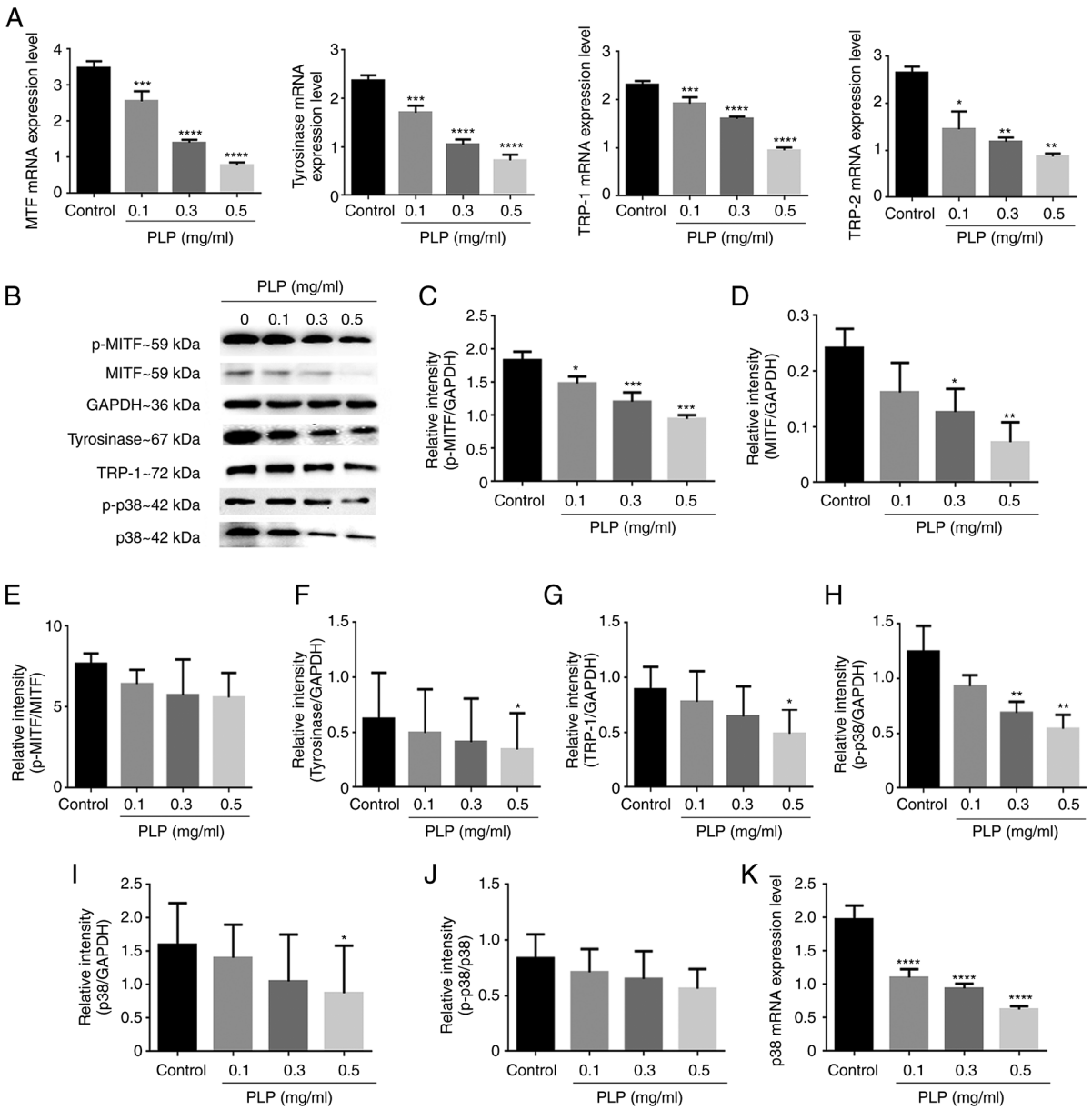

Figure 5. Effects of PLP on melanogenic-related and p38 gene and protein expression levels. (A) The effects of PLP on the mRNA levels of melanogenesis-related genes (MITF, tyrosinase, TRP-1, TRP-2) were detected by reverse transcription-quantitative PCR analysis. (B) Effects of PLP on p-MITF, MITF, tyrosinase, TRP-1, p-p38 and p38 expression levels determined by western blot analysis with GAPDH as an internal reference. (C-J) The protein expression levels of p-MITF, MITF, p-MITF/MITF ratio, tyrosinase, TRP-1, p-p38, p38 and p-p38/p38 ratio. (K) The mRNA level of p38 were detected. Data are expressed as the mean ± SD of three independent experiments. *P<0.05; **P<0.01; ***P<0.001; ****P<0.0001 vs. control. PLP, *P. Lobata* Radix water-soluble total protein extract; MITF, microphthalmia-associated transcription factor; TRP-1, tyrosinase-related protein 1; TRP-2, tyrosinase-related protein 2; p-, phosphorylated.

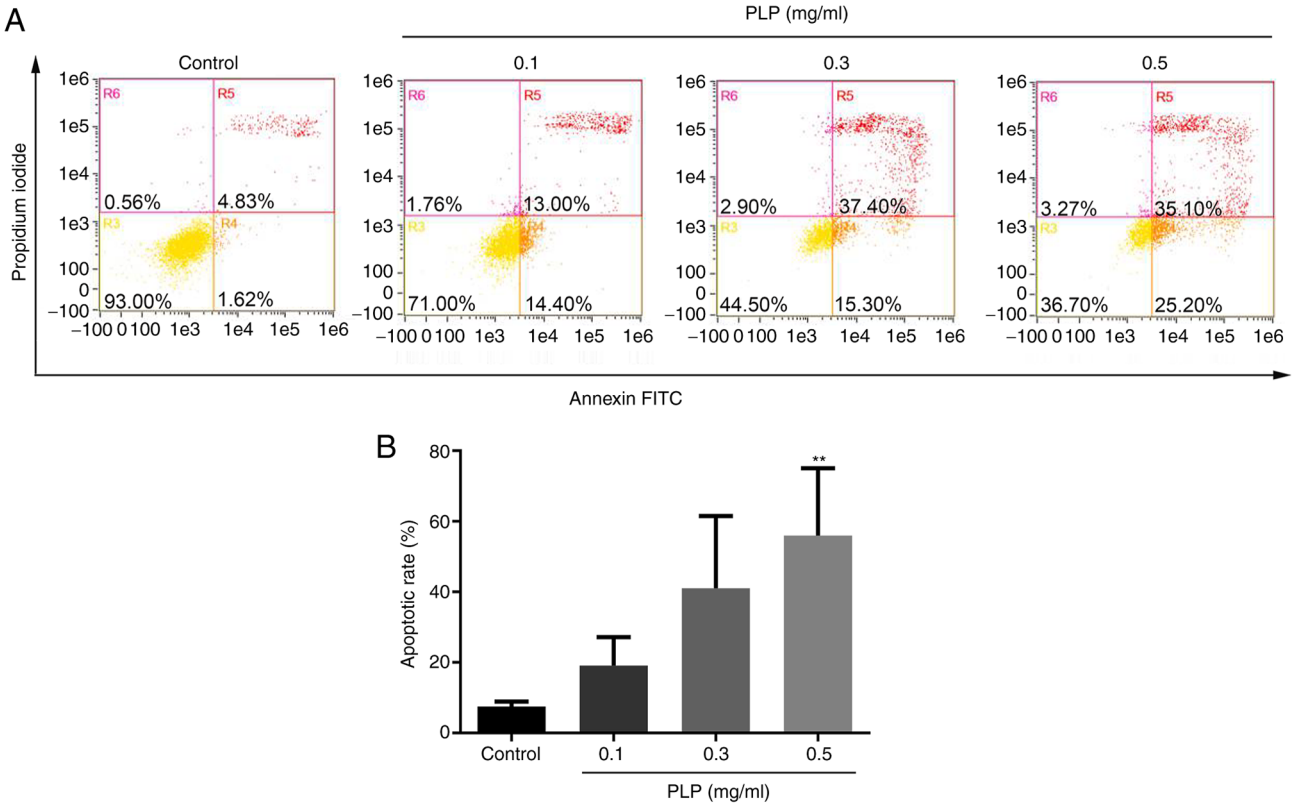

Figure 6. Apoptotic effects of PLP on B16 cells. (A) The treated cells were subjected to flow cytometric analysis after propidium iodide and Annexin V-FITC staining. The total apoptosis ratios included apparent early apoptosis (lower right quadrant) and late apoptosis (upper right quadrant). (B) Percentages of apoptotic B16 cells after treatment with different PLP concentrations. **P<0.01 vs. control. PLP, *P. Lobata* Radix water-soluble total protein extract.

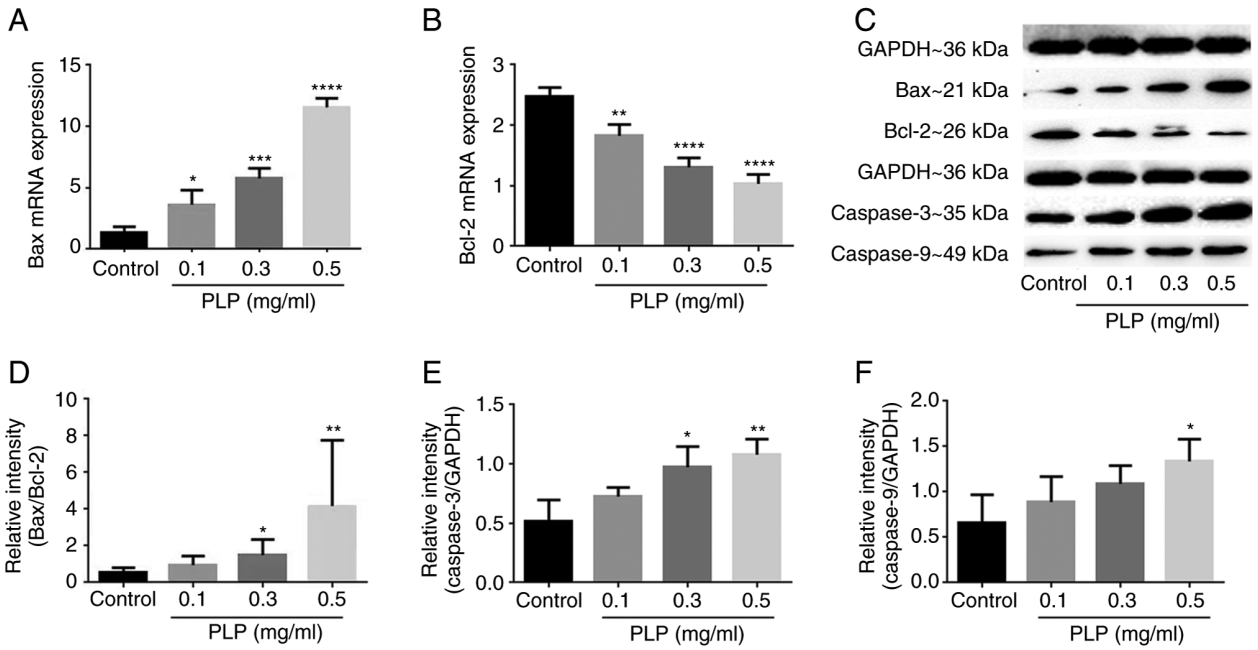

Figure 7. Expression of apoptosis-related proteins and genes. mRNA expression levels of (A) Bax and (B) Bcl-2. (C) Western blot analysis of the expression of apoptosis-related proteins. (D) Bax/Bcl-2 protein ratio quantification. (E) Caspase-3 protein ratio quantification. (F) Caspase-9 protein ratio quantification. *P<0.05; **P<0.01; ***P<0.001; ****P<0.0001 vs. control. Bax, Bcl-2 associated X protein; Bcl-2, B-cell lymphoma-2; PLP, *P. Lobata* Radix water-soluble total protein extract.

B16 melanoma cells, leading to mitochondria-related apoptosis. Cell death induced by PLP was associated with the regulation of mitochondrial energy metabolism, which may explain why MMP collapsed and a reduction in ATP were observed in B16 melanoma cells treated with PLP. Finally, it was demonstrated that the inhibition of melanin synthesis

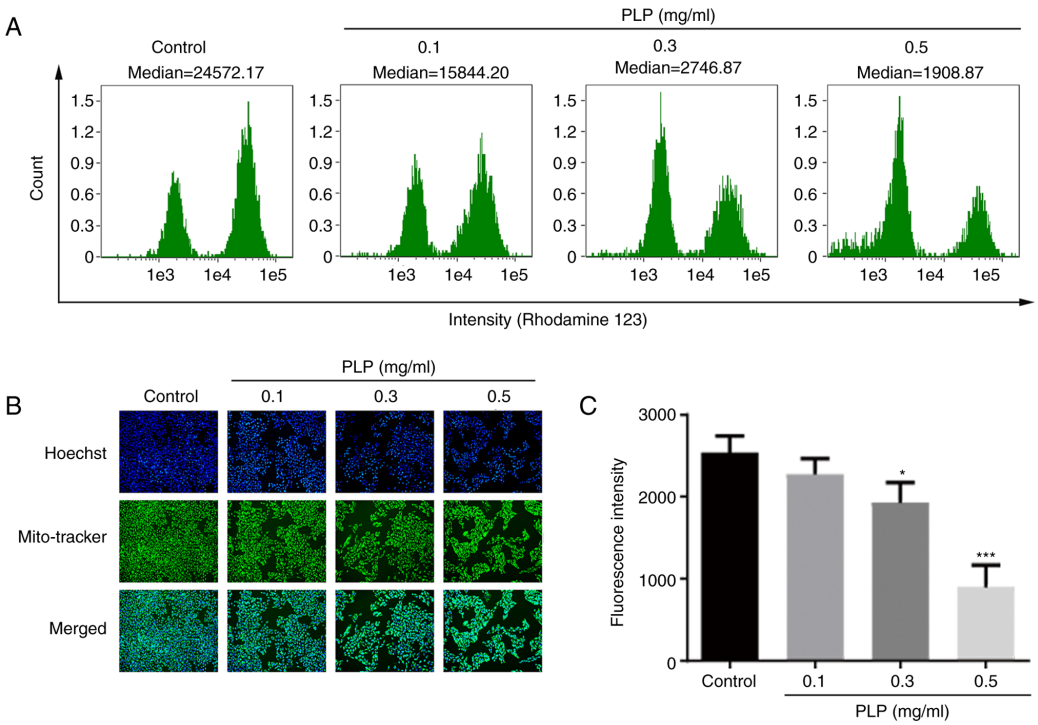

Figure 8. PLP-induced mitochondrial dysfunction in B16 cells. (A) Effects of different concentrations of PLP on MMP in B16 cells. MMP changes are expressed as median values. (B) Monitored changes in MMP of B16 cells by drugs using the Mito-Tracker fluorescent probe method (Magnification=x10; image width=400 μm). (C) Quantitative diagram of fluorescent probe method. *P<0.05; ***P<0.001 vs. control. PLP, *P. Lobata* Radix water-soluble total protein extract; MMP, mitochondrial membrane potential.

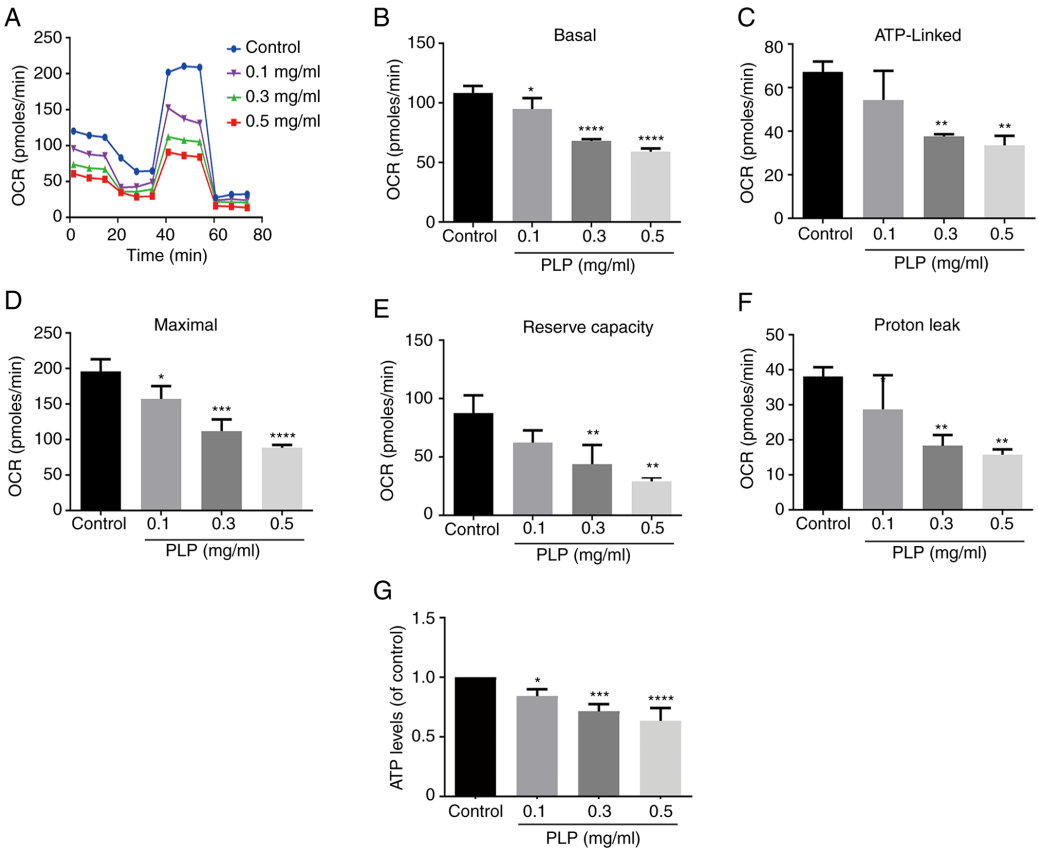

Figure 9. The effect of PLP on mitochondrial energy metabolism and ATP generation. (A) Graphical representation of the OCR measurement over time. (B) Statistical analysis of the basic OCR under the action of PLP. The effects of PLP on the (C) ATP-linked OCR and (D) maximal respiration capacity-linked OCR were calculated from the OCR curves. The effects of PLP on (E) the reserve capacity and (F) proton leak OCR from the OCR curves. (G) Changes in ATP content under the action of PLP. *P<0.05; **P<0.01; ***P<0.001; ****P<0.0001 vs. control. PLP, *P. Lobata* Radix water-soluble total protein extract; OCR, oxygen consumption rate.

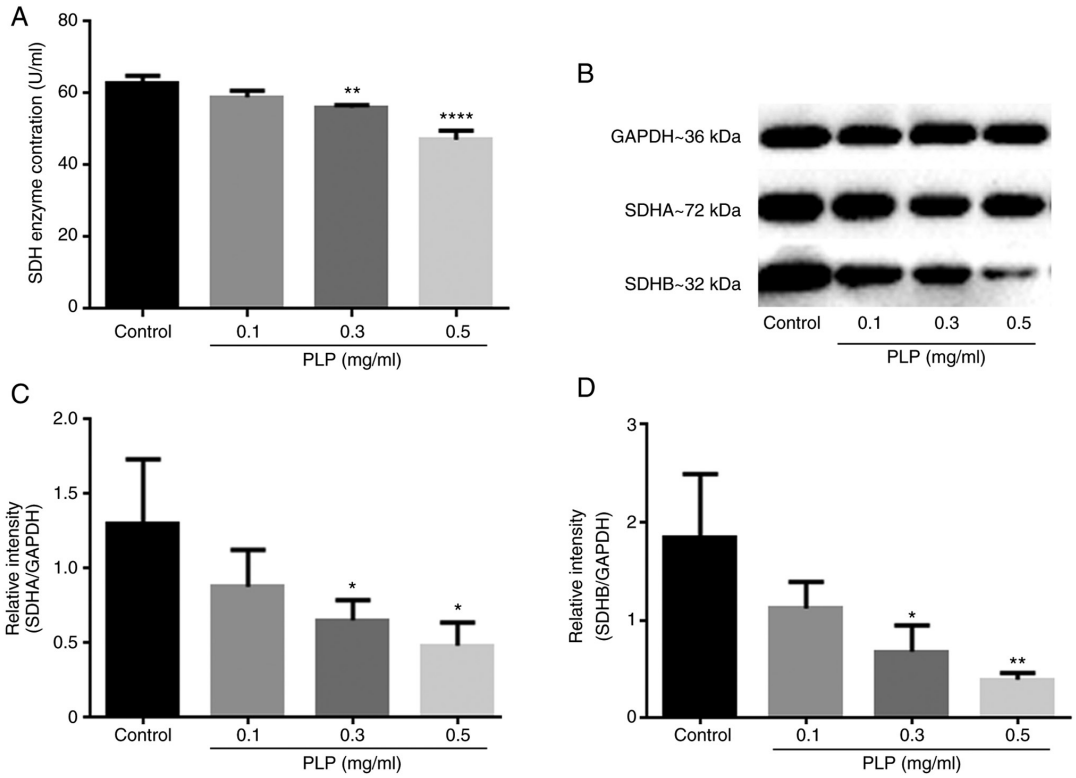

Figure 10. The effect of PLP on SDH. (A) The activity of SDH. (B) Western blot analysis of the expression of succinate dehydrogenase-related protein. Quantification of (C) SDHA and (D) SDHB protein. *P<0.05; **P<0.01; ****P<0.0001 vs. control. PLP, *P. Lobata* Radix water-soluble total protein extract; SDH, succinate dehydrogenase; SDHA, succinate dehydrogenase complex A subunit; SDHB, succinate dehydrogenase complex B subunit.

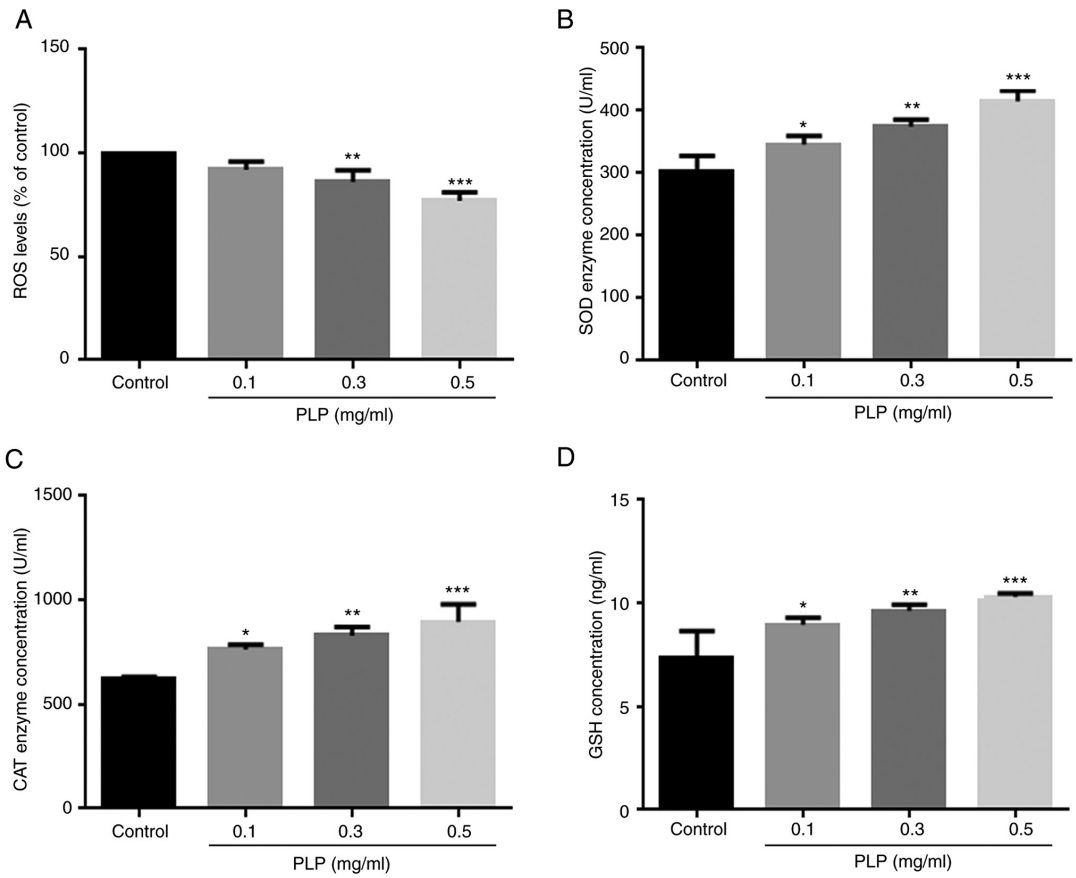

Figure 11. Changes of PLP on oxidative stress-related factors. Measurement of intracellular (A) ROS levels, (B) SOD activity, (C) CAT activity and (D) GSH content. *P<0.05; **P<0.01; ***P<0.001 vs. control. PLP, *P. Lobata* Radix water-soluble total protein extract; ROS, reactive oxygen species; SOD, superoxide dismutase; CAT, catalase; GSH, glutathione.

in B16 cells by PLP was correlated with the regulation of antioxidant enzymes to reduce ROS levels.

Melanogenesis is the process of synthesizing melanin within melanosomes and is a major function of both differentiated normal melanocytes and malignant melanoma cells (28,29). The present study used mouse melanoma cells, as this cell line has been used widely in a number of studies on melanin synthesis (30). It was demonstrated that PLP significantly inhibited the melanin content in B16 cells. A previous study indicated that humans and mice share a number of common genetic features and mice and murine cultured cells are typically used instead of human equivalents in biological experiments (31). A number of reagents have been found to have similar effects on mouse melanoma B16 cells and human epidermal melanocytes (32-35). It was hypothesized that the effects of PLP on melanogenesis in mouse melanoma cells and human melanocytes are likely to be similar, but further research is necessary as animal models provide only an approximation of the situation in humans.

Tyrosinase is the rate-limiting enzyme of melanin biosynthesis in the body (36). Inhibiting the synthesis of tyrosinase and reducing the activity of tyrosinase are effective approaches to reduce melanin synthesis. The extracellular tyrosinase inhibition results for different fractions of *P. Lobata* Radix showed that PLP had the strongest inhibitory effect. The inhibition of tyrosinase by PLP was also studied in melanoma B16 cells and the DOPA-oxidation rate was used as the indicator of inhibition. It was found that treatment with PLP inhibited tyrosinase activity and melanin synthesis in a dose-dependent manner. TRP-1 and TRP-2 are two other key enzymes downstream of tyrosinase that affect melanin biosynthesis (8). The expression of these melanogenic enzymes is affected by MITF (37,38). Therefore, the effect of PLP on the expression of p-MITF, MITF, tyrosinase, TRP-1 and TRP-2 was examined but p-tyrosinase was not evaluated by western blotting which is a limitation of the present study. The expression levels of p-MITF, MITF, tyrosinase, TRP-1 and TRP-2 were inhibited by PLP, indicating that the anti-melanogenesis activity of PLP was produced through downregulation of MITF, which affected the related melanogenic enzymes in melanoma B16 cells. Melanogenesis is regulated by several melanogenic signaling pathways, including p38 MAPK signaling (39). Activation of p38 MAPK increases the expression of MITF and tyrosinase, leading to the induction of melanin synthesis (13). The present study found that p-p38 and p38 were inhibited by PLP, which indicated that the inhibitory effect of PLP on MITF expression was related to p38 MAPK.

MITF is a major regulatory protein for melanocyte growth, differentiation and pigment synthesis and also plays an important role in the malignant transformation of melanocytes and the development and apoptosis of melanocytes. Low levels of MITF can promote cell senescence and ultimately death (40,41). As PLP inhibited MITF expression, whether PLP induced apoptosis of B16 cells was investigated. The results demonstrated that increasing concentrations of PLP enabled stronger cell apoptosis responses. Mitochondria play a key role in the induction of cell apoptosis (42). The mitochondria-related apoptosis pathway is regulated mainly by proteins from the Bcl-2 family, including the anti-apoptotic protein Bcl-2 and the pro-apoptotic protein Bax (43,44). Accumulation of Bax on the mitochondrial outer membrane results in loss of MMP and activation of caspase-9, which activates caspase-3 and causes apoptosis of cells (45,46). Changes in these proteins and decreased MMP were observed in the present study, which indicated that the mitochondrial apoptosis pathway was activated in the PLP-induced apoptosis of melanoma B16 cells. In addition, it was found that the reduction in the MMP was related to a change in the level of SDH on the membrane. SDH directly affects electron transfer in the mitochondrial respiratory chain and thus affects mitochondrial function (47). The activity of SDH and its two subunits, SDHA and SDHB, was determined at the protein level. The content of SDH decreased after treatment with PLP and the levels of the two related subunit proteins decreased simultaneously. Mitochondrial energy metabolism was also evaluated. The results showed that after treatment with PLP, the mitochondrial utilization of oxygen and oxygen consumption were significantly reduced. These results indicated that PLP mediated the mitochondrial apoptotic pathway to inhibit melanoma cell proliferation, thereby reducing melanin synthesis. However, the direct role of MITF in PLP-induced mitochondrial-associated melanoma cell apoptosis induced by PLP needs further characterization.

The over-synthesis of melanin is also related to increases in oxidative stress caused by external stimuli (48,49). ROS have been shown to increase pigmentation (50). Thus, ROS scavengers and inhibitors of ROS production may suppress melanogenesis (51). PLP contains a variety of amino acids, which may be natural antioxidants. PLP reduced the levels of ROS and increased the expression of SOD, CAT and GSH, which indicated a potential antioxidant capacity of PLP. Mitochondria are both the source and target of ROS and excessive or low levels of ROS might disrupt the MMP and induce apoptosis (52-55). Notably, in the present study, mitochondria-associated melanoma B16 cell apoptosis induced by PLP may have been related to a decrease in ROS rather than an increase.

Acknowledgments

Not applicable.

Funding

The present study was supported by the Major Science and Technology Program of Jilin Province (grant no. 20210304002YY).

Availability of data and materials

The datasets used and/or analyzed during the current study are available from the corresponding authors on reasonable request.

Authors' contributions

ML and SW conceived and designed the study; YZ and SY performed experiments; YW, YC and JC collected the data

and confirmed the authenticity of all original data; YZ and JW analyzed the data and prepared the figures; SW, SY and ML drafted and revised the manuscript. All authors read and approved the final manuscript.

Ethics approval and consent to participate

Not applicable.

Patient consent for publication

Not applicable.

Competing interests

The authors declare that they have no competing interests.

References

1. Bonaventure J, Domingues MJ and Larue L: Cellular and molecular mechanisms controlling the migration of melanocytes and melanoma cells. Pigment Cell Melanoma Res 26: 316-325, 2013.
2. Wang HD, Chen CC, Huynh P and Chang JS: Exploring the potential of using algae in cosmetics. Bioresour Technol 184: 355-362, 2015.
3. Otręba M, Rok J, Buszman E and Wrześniok D: Regulation of melanogenesis: The role of cAMP and MITF. Postepy Hig Med Dosw (Online) 66: 33-40, 2012 (In Polish).
4. Otręba M, Miliński M, Buszman E, Wrześniok D and Beberok A: Hereditary hypomelanocytoses: The role of PAX3, SOX10, MITF, SNAI2, KIT, EDN3 and EDNRB genes. Postepy Hig Med Dosw (Online) 67: 1109-1118, 2013 (In Polish).
5. Ahn SJ, Koketsu M, Ishihara H, Lee SM, Ha SK, Lee KH, Kang TH and Kima SY: Regulation of melanin synthesis by selenium-containing carbohydrates. Chem Pharm Bull (Tokyo) 54: 281-286, 2006.
6. D'Mello SA, Finlay GJ, Baguley BC and Askarian-Amiri ME: Signaling pathways in melanogenesis. Int J Mol Sci 17: 1144, 2016.
7. Buitrago E, Hardré R, Haudecoeur R, Jamet H, Belle C, Boumendjel A, Bubacco L and Réglier M: Are human tyrosinase and related proteins suitable targets for melanoma therapy? Curr Top Med Chem 16: 3033-3047, 2016.
8. Pillaiyar T, Manickam M and Namasivayam V: Skin whitening agents: Medicinal chemistry perspective of tyrosinase inhibitors. J Enzyme Inhib Med Chem 32: 403-425, 2017.
9. Wang Y, Li SM, Huang J, Chen SY and Liu YP: Mutations of TYR and MITF genes are associated with plumage colour phenotypes in geese. Asian-Australas J Anim Sci 27: 778-783, 2014.
10. Sun L, Guo Y, Zhang Y and Zhuang Y: Antioxidant and anti-tyrosinase activities of phenolic extracts from rape bee pollen and inhibitory melanogenesis by cAMP/MITF/TYR pathway in B16 mouse melanoma cells. Front Pharmacol 8: 104, 2017.
11. Raja DA, Gotherwal V, Burse SA, Subramaniam YJ, Sultan F, Vats A, Gautam H, Sharma B, Sharma S, Singh A, *et al*: pH-controlled histone acetylation amplifies melanocyte differentiation downstream of MITF. EMBO Rep 21: e48333, 2020.
12. Pathria G, Garg B, Borgdorff V, Garg K, Wagner C, Superti-Furga G and Wagner SN: Overcoming MITF-conferred drug resistance through dual AURKA/MAPK targeting in human melanoma cells. Cell Death Dis 7: e2135, 2016.
13. Jung E, Kim JH, Kim MO, Jang S, Kang M, Oh SW, Nho YH, Kang SH, Kim MH, Park SH and Lee J: Afzelin positively regulates melanogenesis through the p38 MAPK pathway. Chem Biol Interact 254: 167-172, 2016.
14. Wang DD, Jin Y, Wang C, Kim YJ, Perez ZEJ, Baek NI, Mathiyalagan R, Markus J and Yang DC: Rare ginsenoside Ia synthesized from F1 by cloning and overexpression of the UDP-glycosyltransferase gene from bacillus subtilis: Synthesis, characterization, and in vitro melanogenesis inhibition activity in BL6B16 cells. J Ginseng Res 42: 42-49, 2018.
15. Wang S, Zhang S, Wang S, Gao P and Dai L: A comprehensive review on Pueraria: Insights on its chemistry and medicinal value. Biomed Pharmacother 131: 110734, 2020.
16. Hien TT, Kim HG, Han EH, Kang KW and Jeong HG: Molecular mechanism of suppression of MDR1 by puerarin from *Pueraria lobata* via NF-kappaB pathway and cAMP-responsive element transcriptional activity-dependent up-regulation of AMP-activated protein kinase in breast cancer MCF-7/adr cells. Mol Nutr Food Res 54: 918-928, 2010.
17. Xu L, Zheng N, He Q, Li R, Zhang K and Liang T: Puerarin, isolated from *Pueraria lobata* (Willd.), protects against hepatotoxicity via specific inhibition of the TGF-β1/Smad signaling pathway, thereby leading to anti-fibrotic effect. Phytomedicine 20: 1172-1179, 2013.
18. Jeon YD, Lee JH, Lee YM and Kim DK: Puerarin inhibits inflammation and oxidative stress in dextran sulfate sodium-induced colitis mice model. Biomed Pharmacother 124: 109847, 2020.
19. Ye Y, Gao Y, Fang Y, Xu L and He F: Anticancer effect of puerarin on ovarian cancer progression contributes to the tumor suppressor gene expression and gut microbiota modulation. J Immunol Res 2022: 4472509, 2022.
20. Li Y, Zhang C, Ma X, Yang L and Ren H: Identification of the potential mechanism of Radix pueraria in colon cancer based on network pharmacology. Sci Rep 12: 3765, 2022.
21. Zhu J, Xu J, Wang Y, Li C, Chen Z, Song L, Gao J and Yu R: Purification and structural characterization of a novel anti-tumor protein from Arca inflata. Int J Biol Macromol 105: 103-110, 2017.
22. Livak KJ and Schmittgen TD: Analysis of relative gene expression data using real-time quantitative PCR and the 2(-Delta Delta C(T)) method. Methods 25: 402-408, 2001.
23. Noh H, Lee SJ, Jo HJ, Choi HW, Hong S and Kong KH: Histidine residues at the copper-binding site in human tyrosinase are essential for its catalytic activities. J Enzyme Inhib Med Chem 35: 726-732, 2020.
24. Shen XF, Teng Y, Sha KH, Wang XY, Yang XL, Guo XJ, Ren LB, Wang XY, Li J and Huang N: Dietary flavonoid luteolin attenuates uropathogenic Escherichia. Coli invasion of the urinary bladder. Biofactors 42: 674-685, 2016.
25. Bock FJ and Tait SWG: Mitochondria as multifaceted regulators of cell death. Nat Rev Mol Cell Biol 21: 85-100, 2020.
26. Tian L, Zhu C, Yang H, Li Y and Liu Y: Protective effect of mitochondrial ND2 C5178A gene mutation on cell and mitochondrial functions. Oxid Med Cell Longev 2021: 4728714, 2021.
27. Li L, Meng Y, Wu X, Li J and Sun Y: Bromodomain-containing protein 4 inhibitor JQ1 promotes melanoma cell apoptosis by regulating mitochondrial dynamics. Cancer Sci 112: 4013-4025, 2021.
28. Kleszczyński K, Kim TK, Bilska B, Sarna M, Mokrzynski K, Stegemann A, Pyza E, Reiter RJ, Steinbrink K, Böhm M and Slominski AT: Melatonin exerts oncostatic capacity and decreases melanogenesis in human MNT-1 melanoma cells. J Pineal Res 67: e12610, 2019.
29. Orhan IE and Deniz FSS: Inhibition of melanogenesis by some well-known polyphenolics: A review. Curr Pharm Biotechnol 22: 1412-1423, 2021.
30. Sarna M, Krzykawska-Serda M, Jakubowska M, Zadlo A and Urbanska K: Melanin presence inhibits melanoma cell spread in mice in a unique mechanical fashion. Sci Rep 9: 9280, 2019.
31. Dutta S and Sengupta P: Men and mice: Relating their ages. Life Sci 152: 244-248, 2016.
32. Villareal MO, Kume S, Neffati M and Isoda H: Upregulation of Mitf by phenolic compounds-rich cymbopogon schoenanthus treatment promotes melanogenesis in B16 melanoma cells and human epidermal melanocytes. Biomed Res Int 2017: 8303671, 2017.
33. Lee CS, Nam GB and Park JS: Protopanaxatriol inhibits melanin synthesis through inactivation of the pCREB-MITF-tyrosinase signalling pathway in melanocytes. Clin Exp Dermatol 44: 295-299, 2019.
34. Hu Y, Huang J, Li Y, Jiang L, Ouyang Y, Li Y, Yang L, Zhao X, Huang L, Xiang H, *et al*: Cistanche deserticola polysaccharide induces melanogenesis in melanocytes and reduces oxidative stress via activating NRF2/HO-1 pathway. J Cell Mol Med 24: 4023-4035, 2020.
35. Lim HY, Kim E, Park SH, Hwang KH, Kim D, Jung YJ, Kopalli SR, Hong YD, Sung GH and Cho JY: Antimelanogenesis effects of theasinensin A. Int J Mol Sci 22: 7453, 2021.
36. Song W, Zhao YY, Ren YJ, Liu LL, Wei SD and Yang HB: Proanthocyanidins isolated from the leaves of Photinia x fraseri block the cell cycle and induce apoptosis by inhibiting tyrosinase activity in melanoma cells. Food Funct 12: 3978-3991, 2021.

37. Tsatmali M, Ancans J and Thody AJ: Melanocyte function and its control by melanocortin peptides. J Histochem Cytochem 50: 125-133, 2002.
38. Imokawa G: Autocrine and paracrine regulation of melanocytes in human skin and in pigmentary disorders. Pigment Cell Res 17: 96-110, 2004.
39. Sun L, Guo C, Yan L, Li H, Sun J, Huo X, Xie X and Hu J: Syntenin regulates melanogenesis via the p38 MAPK pathway. Mol Med Rep 22: 733-738, 2020.
40. Giuliano S, Ohanna M, Ballotti R and Bertolotto C: Advances in melanoma senescence and potential clinical application. Pigment Cell Melanoma Res 24: 295-308, 2011.
41. Strub T, Giuliano S, Ye T, Bonet C, Keime C, Kobi D, Le Gras S, Cormont M, Ballotti R, Bertolotto C and Davidson I: Essential role of microphthalmia transcription factor for DNA replication, mitosis and genomic stability in melanoma. Oncogene 30: 2319-2332, 2011.
42. Liu WK, Ho JC, Cheung FW, Liu BP, Ye WC and Che CT: Apoptotic activity of betulinic acid derivatives on murine melanoma B16 cell line. Eur J Pharmacol 498: 71-78, 2004.
43. Yang F, Yu Y, Lei Q, Zeng A, Li Y, Xie Y, Ye T and Wei Y: Lobaplatin arrests cell cycle progression, induces apoptosis and impairs migration and invasion in B16-F10 melanoma cell line in vitro. Biomed Pharmacother 69: 402-408, 2015.
44. Li J, Li J, Aipire A, Gao L, Huo S, Luo J and Zhang F: Phenylethanoid glycosides from cistanche tubulosa inhibits the growth of B16-F10 cells both in vitro and in vivo by induction of apoptosis via mitochondria-dependent pathway. J Cancer 7: 1877-1887, 2016.
45. Cartron PF, Bellot G, Oliver L, Grandier-Vazeille X, Manon S and Vallette FM: Bax inserts into the mitochondrial outer membrane by different mechanisms. FEBS Lett 582: 3045-3051, 2008.
46. Yang CC, Hung CF and Chen BH: Preparation of coffee oil-algae oil-based nanoemulsions and the study of their inhibition effect on UVA-induced skin damage in mice and melanoma cell growth. Int J Nanomedicine 12: 6559-6580, 2017.
47. Dalla Pozza E, Dando I, Pacchiana R, Liboi E, Scupoli MT, Donadelli M and Palmieri M: Regulation of succinate dehydrogenase and role of succinate in cancer. Semin Cell Dev Biol 98: 4-14, 2020.
48. Zhang BB, Wang DG, Guo FF and Xuan C: Mitochondrial membrane potential and reactive oxygen species in cancer stem cells. Fam Cancer 14: 19-23, 2015.
49. Wang LX, Qian J, Zhao LN and Zhao SH: Effects of volatile oil from ginger on the murine B16 melanoma cells and its mechanism. Food Funct 9: 1058-1069, 2018.
50. Alfadda AA and Sallam RM: Reactive oxygen species in health and disease. J Biomed Biotechnol 2012: 936486, 2012.
51. Wang J and Yi J: Cancer cell killing via ROS: To increase or decrease, that is the question. Cancer Biol Ther 7: 1875-1884, 2008.
52. Yang S, Zhang Y, Luo Y, Xu B, Yao Y, Deng Y, Yang F, Ye T, Wang G, Cheng Z, *et al*: Hinokiflavone induces apoptosis in melanoma cells through the ROS-mitochondrial apoptotic pathway and impairs cell migration and invasion. Biomed Pharmacother 103: 101-110, 2018.
53. Lu L, Zhang H, Liu J, Liu Y, Wang Y, Xu S, Zhu Z and Xu J: Synthesis, biological evaluation and mechanism studies of C-23 modified 23-hydroxybetulinic acid derivatives as anticancer agents. Eur J Med Chem 182: 111659, 2019.
54. Rizwan H, Pal S, Sabnam S and Pal A: High glucose augments ROS generation regulates mitochondrial dysfunction and apoptosis via stress signalling cascades in keratinocytes. Life Sci 241: 117148, 2020.
55. Yang N, Guan QW, Chen FH, Xia QX, Yin XX, Zhou HH and Mao XY: Antioxidants targeting mitochondrial oxidative stress: Promising neuroprotectants for epilepsy. Oxid Med Cell Longev 2020: 6687185, 2020.